A comprehensive study about the in-cloud processing of nitrate through coupled measurements of individual cloud residuals and cloud water

Guohua Zhang[1,2,3], Xiaodong Hu[1,2,4], Wei Sun[1,2,4], Yuxiang Yang[1,2], Ziyong Guo[1,2,4], Yuzhen Fu[1,2], Haichao Wang[5], Shengzhen Zhou[5], Lei Li[6], Mingjin Tang[1,2,3], Zongbo Shi[7], Duohong Chen[8], Xinhui Bi[1,2,3,*], Xinming Wang[1,2,3]

[1] State Key Laboratory of Organic Geochemistry and Guangdong Provincial Key Laboratory of Environmental Protection and Resources Utilization, Guangzhou Institute of Geochemistry, Chinese Academy of Sciences (CAS), Guangzhou 510640, PR China

[2] CAS Center for Excellence in Deep Earth Science, Guangzhou, 510640, China

[3] Guangdong-Hong Kong-Macao Joint Laboratory for Environmental Pollution and Control, Guangzhou Institute of Geochemistry, CAS, Guangzhou 510640, PR China

[4] University of Chinese Academy of Sciences, Beijing 100049, PR China

[5] School of Atmospheric Sciences, Sun Yat-sen University, Guangzhou 519082, PR China

[6] Institute of Mass Spectrometer and Atmospheric Environment, Jinan University, Guangzhou 510632, PR China

[7] School of Geography, Earth and Environmental Sciences, University of Birmingham, Birmingham B15 2TT, U.K.

[8] State Environmental Protection Key Laboratory of Regional Air Quality Monitoring, Guangdong Environmental Monitoring Center, Guangzhou 510308, PR China

Correspondence to: Xinhui Bi (bixh@gig.ac.cn)

Abstract

While the formation and evolution of nitrate in airborne particles are extensively investigated, little is known about the processing of nitrate in clouds. Here we present a detailed investigation on the in-cloud formation of nitrate, based on the size-resolved mixing state of nitrate in the individual cloud residual and cloud-free particles obtained by single particle mass spectrometry, and also the mass concentrations of nitrate in the cloud water and $PM_{2.5}$ at a mountain site (1690 m a.s.l.) in southern China. The results show a significant enhancement of nitrate mass fraction and relative intensity of nitrate in cloud water and the cloud residual particles, respectively, reflecting a critical role of in-cloud processing in the formation of nitrate. We first exclude the gas phase scavenging of HNO_3 and the facilitated activation of nitrate-containing particles as the major contribution for the enhanced nitrate, according to the size distribution of nitrate in individual particles. Based on regression analysis and theoretical calculations, we then highlight the N_2O_5 hydrolysis for the in-cloud formation of nitrate, even during the daytime, attributed to the diminished light in clouds. Nitrate is highly related (R^2 = ~0.6) to the variation of $[NO_x][O_3]$, temperature and droplet surface area in clouds. Accounting for droplet surface area greatly enhances the predictability of the observed nitrate, compared with using $[NO_x][O_3]$ and temperature. The substantial contribution of N_2O_5 hydrolysis to nitrate in clouds during the daytime was reproduced by a multiphase chemical box model. Assuming a photolysis rate at 30% of the default setting, the overall contribution of N_2O_5 hydrolysis pathway to nitrate formation increases by ~20% in clouds. Given that N_2O_5 hydrolysis acts as a major sink of NO_x in the

atmosphere, further model updates would improve our understanding about the processes contributing to nitrate production in cloud and the cycling of odd nitrogen.

1. Introduction

Aerosol nitrate is an increasingly important component of $PM_{2.5}$, in particular, contributing to haze formation in China (Liu et al., 2020b; Xu et al., 2019; Zheng et al., 2020; Fu et al., 2020; Guo et al., 2014; Tian et al., 2019; Wen et al., 2018; Lu et al., 2019). As a key inorganic component in cloud water, nitrate can also modify microphysical properties of cloud, influence aqueous-phase processes in droplets and affect ecosystem after wet deposition (Schneider et al., 2017). Notably, aerosol nitrate is an important product in the cycling of odd nitrogen (Chang et al., 2011; Zheng et al., 2020; Zhang et al., 2021; Huang et al., 2018), playing significant roles in tropospheric ozone and OH production (Scharko et al., 2014; Kaur and Anastasio, 2017; Ye et al., 2017a; Ye et al., 2017b), and contributing to net aerosol composition and radiative forcing (Bauer et al., 2007; Hauglustaine et al., 2014; Xu and Penner, 2012).

Aerosol nitrate originates from the oxidation of NOx, which refers to gas phase oxidation of NO_2 by the hydroxyl radical (OH) followed by condensation (daytime chemistry) and the hydrolysis of N_2O_5 (nighttime chemistry) to nitrate in aqueous particles, initiated by the oxidation of NO_2 by ozone (O_3) to produce the NO_3 radical (Seinfeld and Pandis, 2006). In contrary to aerosol sulfate formation, which is dominated by aqueous phase reactions, both gas phase oxidation and the hydrolysis of N_2O_5 represent the major processes forming aerosol nitrate (Hayden et al., 2008; Sellegri et al., 2003; Fahey et al., 2005; Chen et al., 2020; Xiao et al., 2020). Extensive studies have shown that the formation and evolution of nitrate depend on various factors, such as the availability of ammonia (NH_3), temperature

(T), relative humidity (RH), and the presence of other ionic species in particulate phase (Chen et al., 2018; Shi et al., 2019; Chen et al., 2020; Lin et al., 2021; Fan et al., 2021).

Comparatively, detailed observational investigations and the possible mechanisms governing nitrate behavior upon in-cloud processes are scarce and poorly understood, although it is well-known that clouds play an important role in the transport and transformation of tropospheric pollutants (Li et al., 2020b; Ervens, 2015; McNeill, 2017). Global model studies still disagree on the relative importance of in-cloud process contributing to the production of HNO_3. While most have neglected N_2O_5 and NO_3 uptake in clouds (Alexander et al., 2009; Hauglustaine et al., 2014; Xu and Penner, 2012), there is also research suggesting the significance of in-cloud process (Holmes et al., 2019). Likewise, despite limited research, the role of clouds in nitrate formation from field observations remains controversial. Drewnick et al. (2007) and Prabhakar et al. (2014) reported that the relatively enhanced nitrate in clouds was associated with the composition of the activating cloud condensation nuclei (CCN), rather than preferential scavenging of nitric acid (HNO_3) in clouds. Differently, there are also studies highlighting the predominant role of nitric acid partitioning in nitrate formation in clouds, in contrary to nucleation scavenging of sulfate (Schneider et al., 2017; Hayden et al., 2008; Leaitch et al., 1988). Hayden et al. (2008) also noted that potential contributions from gas-phase N_2O_5 cannot be ruled out. Therefore, more detailed information on the pathways of nitrate and controlling factors in cloud are still required for models to further integrate the role of cloud in the formation of nitrate in the troposphere (Zhu et al., 2020; Wu et al., 2021).

The aim of this study is to illustrate the in-cloud formation mechanisms of nitrate and evaluate the relative contribution of each pathway to nitrate in cloud water for daytime and nighttime. To this aim, the mixing state of individual cloud residual, interstitial and cloud-free particles were measured in high-time resolution with a single particle aerosol mass spectrometer (SPAMS). The combination of a counter flow virtual impactor (CVI) and aerosol mass spectrometry (including SPAMS) allows for the high-time resolved observations of size and chemical compositions of submicron cloud residual particles (Boone et al., 2015; Hao et al., 2013; Zhang et al., 2017; Lin et al., 2017). In addition, cloud water and $PM_{2.5}$ samples were collected, and the chemical compositions were measured to provide additional quantitative evidence.

2. Experimental section

2.1 Aerosol and cloud measurements

Aerosol and cloud measurements were performed at the Mt. Tianjing site (24°41′56″N, 112°53′56″E, 1690 m a.s.l.) in southern China, as described in detail by Lin et al. (2017), during 9 May – 4 June 2018 and 13 November – 9 December 2020. Cloud events can be distinguished by a sudden drop of visibility (to < ~1 km) and a sharp increase of RH to > 95%, as record by sensors equipped with a ground-based counterflow virtual impactor (GCVI) (Model 1205, Brechtel Mfg. Inc., USA) (Lin et al., 2017). Overall, nineteen cloud events (lasting more than six hours) were identified for 2018 spring and ten for 2020 winter, as also marked in Fig. S1. The visibility was generally lower than 0.1 km during the cloud

events, versus as high as 80 km during the cloud-free periods. Besides a relatively long cloud event throughout 9 – 12 May, the cloud events were typically observed during nighttime for 2018 spring, associated with a prominently diurnal variation of RH and visibility. The RH during the daytime ranged between 70-80%, and raised to > 95% during nighttime. The duration of cloud events was in a range of 6-24 hours for 2020 winter. Air masses from the southern continental and marine areas dominated over the 2018 spring and 2020 winter periods, with air masses from western continental areas unique for the 2020 winter (Fig. S2), obtained by HYSPLIT 4.9 (http://ready.arl.noaa.gov/HYSPLIT.php) (Draxler and Rolph, 2012).

An incorporation of counterflow virtual impactor (CVI) or GCVI allows the separation of interstitial gases and aerosols from cloud droplets that are evaporated to obtain the cloud residual particles (Bi et al., 2016; Roth et al., 2016; Pratt et al., 2009). Briefly, the GCVI was applied to collect the cloud droplets with predefined size (7.5-8.5 μm in the present study), with the cloud residual particles as output after dried in the evaporation chamber (with an air flow temperature at 40 °C) (Shingler et al., 2012). The influence of cloud-free air can be negligible as the number concentration of GCVI output particles was measured to be ~1 cm^{-3}, but at a magnitude of ~10^3 cm^{-3} in the cloud-free air. In the present study, the average number concentration of the cloud residual particles sampled during the cloud events was at a level of ~100 cm^{-3}. In addition, a $PM_{2.5}$ inlet was used to deliver cloud interstitial particles during cloud events or cloud-free particles.

2.2 SPAMS measurements and data processing

A SPAMS (Hexin Analytical Instrument Co., Ltd., Guangzhou, China), an Aethalometer (AE-33, Magee Scientific Inc.), and a scanning mobility particle sizer (SMPS; MSP Cooperation) were deployed to characterize the physical and chemical properties of the sampled particles. The instruments were connected downstream the GCVI or $PM_{2.5}$ inlets. Cloud residual and cloud interstitial particles were alternately sampled with an interval of ~1 h during some randomly selected cloud events. During the cloud free period, these instruments were connected to the $PM_{2.5}$ inlet in order to measure the cloud-free particles. In the present study, aerosol surface area (SA) for the cloud-free particles were directly calculated from the size distribution data obtained from the SMPS, whereas it can only be estimated based on the same data for the cloud residues assuming a mean droplet size at 8 μm. We recognize the possible uncertainty, but the estimated SA should linearly correlate with real values and thus would not lead to ambiguous conclusions.

The vacuum aerodynamic diameter (d_{va}) and mass spectral information for individual particles were measured by the SPAMS (Li et al., 2011). A brief description on the performance of the SPAMS can also be found in the Supplement. Over the sampling period for the 2018 spring and 2020 winter periods, a respective ~20, 000, 000 particles with mass spectral information were analyzed, using the FATEs toolkit based on Matlab (The MathWorks, Inc.) (Sultana et al., 2017). The particles were classified by an adaptive resonance theory-based neural network algorithm (Song et al., 1999), with the inputs of ion peak intensities. Seven types with distinct mass spectral characteristics (Fig. S3), accounting

for > 95% of all the detected particles, were obtained for further analysis. The presence of nitrate can be identified with ion peaks (defined as five times the noise signal) at m/z -62 $[NO_3]^-$ or m/z -46 $[NO_2]^-$. Approximate 70-80% of all the detected particles in the size range of 100-2000 nm contained nitrate ion signals for our measurements. Defined as fractional peak area of each m/z relative to the sum of peak areas in a mass spectrum, relative peak area (RPA) is applied to represent the relative amount of a species within a particle (Jeong et al., 2011; Healy et al., 2013).

2.3 Cloud water/$PM_{2.5}$ collection and chemical analysis

A Caltech Active Strand Cloud Water Collector (CASCC2) was applied to collect cloud water (with droplet size > 3.5 μm). The average cloud liquid water content (LWC) for each sampling period can be derived from $LWC = \Delta m / (\Delta t \times \eta \times Q)$, based on each sample mass (Δm), duration time (Δt), flow rate ($Q = 5.8\ m^3\ min^{-1}$), and collection efficiency (η = 86%).

A total of 58 / 53 cloud water samples were collected over the nineteen / ten cloud events for 2018 spring and 2020 winter periods, respectively, with the durations ranging between 2 and 10 hours. The pH for collected samples were immediately measured using a pH meter (Mettler Toledo, Switzerland) after filtered through a 0.22 μm filter, followed by kept at -20 ℃ until the analysis.

$PM_{2.5}$ samples were collected on quartz filters using a $PM_{2.5}$ sampler (PM-PUF-300, Mingye Instruments, China) at a flow rate of 300 L min^{-1}. The filter were pre-conditioned in 450 ℃ for 6 hours to eliminate the potential influence of organics. A total of 20 / 36 $PM_{2.5}$

samples were collected for the 2018 spring and 2020 winter periods, respectively. The samples were kept at -20 ℃ immediately until further analysis. These samples are representative for the cloud-free particles or cloud interstitial particles during cloud events.

Cloud water and $PM_{2.5}$ samples were analyzed with ion chromatograph (Metrohm 883 IC plus, Switzerland) for water soluble inorganic ions (Na^+, NH_4^+, K^+, Ca^{2+}, Mg^{2+}, Cl^-, NO_3^-, and SO_4^{2-}) and total organic carbon analyzer (Vario, Elementar, Gemany for 2018 samples and TOC-V, Shimadzu, Japan for 2020 samples) for water soluble organic carbon (WSOC). The overall uncertainty for the concentration of each species is calculated to be < 15% based on parallel analyses. The nitrate mass fractions in cloud water and $PM_{2.5}$ were calculated by dividing the nitrate concentration by the sum of the measured water-soluble inorganic ions and water-soluble organic matter (estimated by 1.6*WSOC).

2.4 Box modeling of nitrate formation in cloud

A multiphase chemical box model (RACM-CAPRAM) was used to simulate the production of nitrate in wet aerosols and cloud droplets. It couples the regional atmospheric chemistry mechanism version 2 (RACM2; including 363 chemical reactions) and the chemical aqueous-phase radical mechanism version 2.4 (CAPRAM2.4; including 438 chemical reactions) to account for gas- and aqueous-phase atmospheric chemistry (Ervens et al., 2003). As similarly performed in previous studies (Pathak et al., 2009; Wen et al., 2018), three major pathways for nitrate formation are considered: (1) The oxidation of NO_2 by the OH radical produces HNO_3 and partitioning of gaseous HNO_3 into the aqueous phase;

195 (2) The hydrolysis reactions of N_2O_5; and (3) The aqueous-phase reactions of NO_3 radicals.

196 The average concentration of NO_2 (~25 ppb) and O_3 (~100 ppb) for gas-phase precursors

197 and LWC (0.1 g m^{-3}) for cloud droplets, obtained from the in-situ measurements, were taken

198 as representative parameters for the atmosphere condition at Mt. Tianjing, and used as initial

199 conditions for model simulation. The detailed initial conditions for the model are listed in

200 the SI Table S1. Several comparisons through varying the LWC and photolysis rate were

201 considered in order to investigate the role of LWC and photolysis on the formation of nitrate

202 in the cloud. It is also noted that only LWC and photolysis rate were reset in our scenario,

203 with other factors (e.g., initial droplet composition, SO_2) kept as default setting in the model

204 setup.

205

206 **3. Results and discussion**

207 **3.1. Enhanced in-cloud production of nitrate**

208 Figure 1 shows the statistical results of the nitrate mass fractions in cloud water and

209 $PM_{2.5}$ and the hourly average relative intensity of nitrate (represented by the RPA) in the

210 cloud-free, cloud residual, and cloud interstitial particles. The results clearly indicate the

211 enhancement of nitrate in clouds. It can be seen that the mass fraction of nitrate in cloud

212 water (~20% on average) is obviously higher than those in $PM_{2.5}$ (< 15% on average) during

213 the cloud-free periods and cloud events, for both the 2018 spring and 2020 winter periods.

214 Consistently, the relative intensity of nitrate was substantially enhanced in the cloud

215 interstitial particles and particularly cloud residues, relative to the cloud-free particles. The

influence of air mass on the enhanced nitrate can be ruled out for the 2018 spring period, as they similarly originated from southern areas over the whole campaign period (Fig. S2). While the air masses originated from different regions during the 2020 winter period, they did not show the difference between the cloud-free periods and cloud events, with the shifting of air masses and/or wind direction after 27 Nov (Figs. S1 and S2). Thus, the influence of air mass on the enhanced nitrate in 2020 winter should also be limited.

There are several pathways that might contribute to the enhanced nitrate in cloud droplets, including (1) the scavenging of gas-phase HNO_3, (2) the preferential activation of nitrate-rich particles, and (3) in-cloud aqueous production of nitrate via reaction of NO_3 radicals or hydrolysis of N_2O_5. The mechanism via the dissolution of NO_2 and its aqueous phase oxidation is relatively slow and unlikely to be a significant source of cloud water nitrate (Seinfeld and Pandis, 2006).

We first exclude the scavenging of gas-phase HNO_3 as a major pathway through the analysis of size distribution of nitrate RPA and RPA ratio (nitrate / sulfate), although all the gas phase HNO_3 could be efficiently scavenged and present in the aqueous phase in a typical cloud with LWC > 0.1 g m^{-3} (Seinfeld and Pandis, 2006). As can be seen in Fig. 2, the RPA of nitrate and RPA ratios of nitrate to sulfate distributes relatively stable over the measured size range, which suggests that the gas phase scavenging of HNO_3 is not the dominant pathway in the present conditions. This is because gas-phase mass transfer would lead to enhanced nitrate in the smaller droplets with higher total surface area (Drewnick et al., 2007). Comparatively, the limited size dependence of nitrate for the cloud RES particles differs

markedly from that observed by Hayden et al. (2008), showing a favorable presence of nitrate in smaller size, rather than sulfate in larger size. And their pattern could be well explained by the model calculation assuming that all of the cloud nitrate comes from the uptake of HNO_3. Therefore, our pattern at least indicates a limited contribution of gas-phase scavenging of HNO_3 to the observed nitrate in the cloud RES particles. As also discussed in the following section, the formation of HNO_3 would be certainly suppressed by the presence of cloud.

We also indicate that the contribution of preferential activation of the nitrate-rich particles should be limited since such a process would lead to the depletion of nitrate in the cloud interstitial particles relative to the cloud-free particles. But this is not the case, as the RPA of nitrate and RPA ratios of nitrate to sulfate in the cloud interstitial particles are considerably higher than those in the cloud-free particles (Fig. 2). Both the enhanced nitrate in the cloud residual and interstitial particles suggest the in-cloud formation of nitrate, although the variation of nitrate RPA cannot provide a quantitative view. The enhancement of nitrate in the cloud interstitial particles may also indicate that the significant role of RH in the formation of nitrate, even in the inactivated particles. Similar results have also been observed in our previous study for oxalate (Zhang et al., 2017). Consistently, the formation of nitrate in the cloud interstitial particles also grows their size towards the larger mode, compared with the cloud-free particles (Fig. S4).

3.2. In-cloud nitrate formation

A theoretical estimation of nitrate production for 2020 winter is performed based on the well-established kinetic characteristic of reactions between NO_2 and O_3 and uptake of N_2O_5 onto aerosol/droplet surfaces that formed HNO_3 (SI text S1), corresponding to the nighttime chemistry. It is reasonable since the heterogeneous hydrolysis of N_2O_5 within aerosol particles, fog, or cloud droplets has been shown to be much faster than homogeneous hydrolysis under typical tropospheric conditions (Chang et al., 2011; Wang et al., 2017). Through integrating the rate equations, as listed in SI text S1, the solution for aqueous phase production of HNO_3 can be obtained (Seinfeld and Pandis, 2006):

$$[\mathrm{HNO_3}] = \frac{[\mathrm{NO}_x]}{2}\left\{1 + \frac{1}{\tau_{NO_x} - \tau_{N_2O_5}}\left[\tau_{N_2O_5}\exp\left(-\frac{t}{\tau_{N_2O_5}}\right) - \tau_{NO_x}\exp\left(-\frac{t}{\tau_{NO_x}}\right)\right]\right\}$$

Thus, the conversion of NOx to HNO_3 through the hydrolysis of N_2O_5 depends on the two lifetimes τ_{NO_x} and $\tau_{N_2O_5}$, as defined by the reaction kinetics (SI text S1). The key reaction that formed aqueous phase nitrate is related to the effective reaction of N_2O_5 on the surface of wet aerosol or droplets (Holmes et al., 2019), and therefore, depends on the concentration of NO_2 and O_3 ($[NO_2][O_3]$), the available aerosol and droplet SA, and temperature. Besides the reaction kinetics, temperature could also have influence on the hydrolysis of N_2O_5 (Chen et al., 2018; Chang et al., 2011).

As shown in Fig. 3, the theoretically calculated in-cloud nitrate production assuming a typical uptake coefficient of N_2O_5 $\gamma = 0.06$ (Seinfeld and Pandis, 2006) could well match the measured nitrate concentrations well (with $R^2 = 0.38$ and 0.60 at $p < 0.01$ for daytime and nighttime, respectively), varying in a wide range of ~1 mg L^{-1} to ~60 mg L^{-1} for 2020 winter. The correlation coefficients are obviously higher than those predicted using only $[NOx][O_3]$

279 (with R^2 = 0 and 0.54 for daytime and nighttime, respectively). This is consistent with
280 previous results that the nighttime production of N_2O_5 and HNO_3 would be proportional to
281 the concentration of NO_2 and O_3 ([NO_2][O_3]) when assuming N_2O_5 and the NO_3 radical are
282 both in steady state considering their short lifetimes (Li et al., 2018; Wang et al., 2017). The
283 result also highlights the significance of SA in the in-cloud N_2O_5 hydrolysis in the build-up
284 of nitrate through in-cloud processing, even during the daytime. A further comparison of
285 [NOx][O_3] and SA for the cloud events and cloud free periods, as shown in Fig. S5, also
286 supports the above discussion that the higher fraction of nitrate cannot be well explained by
287 the variations of [NOx][O_3], but rather by the enhanced SA due to the presence of droplets
288 (Fig. S5b), which is > 5 times on average that for aerosol particles during cloud-free periods.
289 In the present study, the average LWC of cloud droplets is at a level of ~10^5 μg m^{-3}, 3-4
290 magnitude higher than those for urban haze conditions. As previously reported, high aerosol
291 LWC (campaign average at ~50 μg m^{-3}) induced fast heterogeneous uptake of N_2O_5 (γ =
292 0.048 on average) is prevalent in urban haze (Wang et al., 2017), compared with $\gamma < 0.03$ for
293 normal periods, and thus results in enhanced nitrate in highly humid condition (Neuman et
294 al., 2003; Wang et al., 2009; Pathak et al., 2009)."

295 The theoretical estimate indicates that the hydrolysis of N_2O_5 may substantially
296 contribute to the in-cloud production of nitrate even during the daytime, consistent with the
297 observation results as discussed in Section 3.1. The theoretically predicted nitrate (NO_3^-)
298 production from the hydrolysis of N_2O_5 represents ~5-15% of the measured nitrate (Fig. 3)
299 based on our assumption. It could roughly explain ~10% increase of the nitrate mass fraction

in clouds (Fig. 1). There are some factors that may contribute to the uncertainties in the estimation. One is that the assumed $\gamma = 0.06$ might not be representative for N_2O_5 uptake in cloud droplets, since the previously reported γ varies in a wide range, depending on various factors (e.g., droplet compositions, pH, temperature) (Bertram and Thornton, 2009; Holmes et al., 2019; Burkholder et al., 2015). Some higher γ (0.2-0.4) was also observed for deliquescent sodium sulfate particles (Burkholder et al., 2015). Another is that the SA estimated by the size distribution data of cloud residues obtained by the GCVI-SMPS only represents part (< 50%) of the cloud droplets, as GCVI was set to collect droplets larger than 7.5 μm in the present study. In addition, the scavenging of HNO_3 may still contribute to the in-cloud nitrate production, as estimated in section 3.3, although N_2O_5 hydrolysis still represents the dominant pathway.

Furthermore, a simplified regression and a random forest analysis are also performed for the high-time resolved RPAs of nitrate obtained by the SPAMS, with $[NOx][O_3]$, SA, and temperature as inputs, separated for the cloud RES and cloud-free particles, as detailed in SI text S2. Note that the concentration of NOx is used here to represent that of NO_2, since most of NO data were not available for the 2018 spring. The effect should be limited since NO could be negligible when the air masses are dominantly attributed to long range transport, which could also be supported by the data (NO, ~0.1 μg m^{-3}, < 2% of NO_2 concentration) in 2020 winter. As expected, the nitrate RPA in the cloud residual particles is highly correlated to the predicted ones (R^2 = 0.75 and 0.71 with $p < 0.01$ for the daytime and nighttime, respectively), even during the daytime (**Fig. 4**). An inclusion of temperature and SA in the

model substantially improves the correlation coefficient R^2, which is originally 0.16 and 0.31 between the nitrate RPA and [NOx][O_3] for the daytime and nighttime, respectively. Similarly, the correlation coefficients (R^2 = 0.45 and 0.66 for daytime and nighttime, respectively) are lower for 2018 spring than 2020 winter, without the availability of SA data. The results are generally consistent with those obtained from random forest analysis, as shown in Fig. S6. Without the input of SA, [NOx][O_3] and temperature only explains 52-61% of the observed nitrate RPA for cloud residual particles in 2018 spring, compared with 72-80% in 2020 winter. Compared with the cloud residual particles, the predictions for the nitrate RPA in the cloud-free particles are of lower coefficients. Such difference between the cloud residual and cloud-free particles also reflects the critical role of SA in the hydrolysis of N_2O_5 in cloud droplets.

3.3. Relative importance of N_2O_5 hydrolysis pathway to nitrate in clouds

The relative contribution of nitrate formation in the cloud droplets and cloud-free particles is also assessed using the CAPRAM model, as shown in Fig. 5. The relative contribution difference between the cloud droplets and cloud-free particles is primarily attributed to the different LWC setting, which is tightly linked to the cloud droplets' SA. Furthermore, the comparison between cloud scenarios with different LWC setting (0.05 g m^{-3} versus 0.15 g m^{-3}) also shows an enhanced contribution of N_2O_5 hydrolysis to nitrate with increasing LWC.

Nitrate is known to form predominantly by the hydrolysis of N_2O_5 (> 80%) for both the

cloud droplets and cloud-free particles for the nighttime. However, both Fig. 3 and Fig. 4 indicate the potential importance of the heterogeneous N_2O_5 hydrolysis to nitrate formation during the daytime. This is likely attributed to the substantial attenuation of the incident solar radiation by clouds, in which the visibility was as low as < 0.1 km over this study. Previous studies have also indicated the effect of clouds in the vertical redistribution of the photochemical activity (Liu et al., 2006; Hall et al., 2018). Most comparatively, Brown et al. (2016) observed a discrepancy between the modelled and observed N_2O_5 during a daytime fog episode in Hong Kong, and attributed to the uptake of N_2O_5 to fog droplets. Their calculation infers that daytime production of soluble nitrate via N_2O_5 can be substantially faster than photochemical conversion through OH + NO_2 in the polluted fog episodes (Brown et al., 2016). One may expect that the substantial attenuation of the incident solar radiation by clouds may inhibit the formation of O_3, thereby affecting the formation of N_2O_5. However, the concentration of O_3 showed relatively stable and limited variations throughout the cloud events (Fig. S1). Together with the similar [NOx][O_3] observed during the cloud events and cloud-free periods (Fig. S5), we indicate that the cloud events did not have much effect on the variation of O_3 during our observation.

The model results in Fig. 5 with the consideration of photolysis rate are, to some extent, consistent with our observations. The overall contribution of N_2O_5 hydrolysis pathways increases by ~20% (from ~50-60% to ~70-80%) when the photolysis rate is reduced to 30% of the default setting. For daytime only, the contribution of this pathway also increases from nearly 0 to ~20% during the noon hours and ~40% for the morning hours. A similar model

study also indicates that N_2O_5 hydrolysis contributed to 30% of daytime nitrate formation at Mt. Tai (Zhu et al., 2020). Attributed to the substantial attenuation of incident solar radiation by clouds and high loading of $PM_{2.5}$, the daytime N_2O_5 hydrolysis has also been observed to be an important formation pathway for nitrate in the haze episodes in Xi'an (China), and the contribution increases from 8.2% to 20.5% of the total nitrate over 14:00–16:00 by model simulation (Wu et al., 2021). Similarly, Liu et al. (2020a) showed that the daytime N_2O_5 hydrolysis contributed to ~10% of nitrate in the north China plain in winter. Note that biogenic volatile organic compounds could also have a potentially important impact on nitrate formation through reacting with NO_3 radical, which may lead to up to 35% decrease of particulate nitrate (Fry et al., 2014; Aksoyoglu et al., 2017). However, the modelling results could still indicate the role of cloud in the hydrolysis of N_2O_5, which contributes to the enhanced nitrate.

4. Conclusions and atmospheric implications

The presented results provide direct evidence that in-cloud aqueous processing, in particular, the hydrolysis of N_2O_5 significantly contributes to the enhanced nitrate in cloud residues. We highlight that the hydrolysis of N_2O_5 serves as the critical route for the in-cloud formation of nitrate, even during the daytime. The dependence of in-cloud nitrate formation on the cloud droplets' SA extends the observation fact that higher RH facilities the formation of nitrate in wet aerosols (Neuman et al., 2003; Wang et al., 2009; Pathak et al., 2009). Given that N_2O_5 hydrolysis acts as a major sink of NOx in the atmosphere (Yan et al., 2019), further

model updates may improve our understanding of the relative importance of nitrate-production pathways (Chan et al., 2021; Alexander et al., 2020). In addition, significant hydrolysis of N_2O_5 in cloud may also pose substantial effect on the tropospheric ozone budget (Riemer et al., 2003; Voulgarakis et al., 2009; Strode et al., 2017).

As sulfate is reduced in the future through emission controls (Li et al., 2020a; Chu et al., 2020), higher nitrate fraction is expected in cloud (Herckes et al., 2007; Herckes et al., 2015). However, the limited dependence of nitrate formation on the [NOx][O_3] in the cloud suggest a possibility that controlling NOx and O_3 might be offset in the cloudy regions. Given the significance of both emission and deposition on the variations of nitrate (Zhai et al., 2021) and the contribution of the transported NOx and O_3 to the notable effect and complex process of cross-regional nitrate formation (Qu et al., 2021), knowledge of the in-cloud formation of nitrate would also benefit $PM_{2.5}$ pollution control target over a larger scale.

Furthermore, our results indicate that in-cloud formed nitrate remains in particulate phase after cloud evaporation (Fig. S7), changing the mixing state of individual particles. Enhanced aerosol nitrate is expected to have higher hygroscopicity after cloud evaporation (Sun et al., 2018; Hodas et al., 2014), and therefore, an increase of the particles' ability to act as cloud condensation nuclei after their cloud passage (Roth et al., 2016). This is different from that observed in California coast that the nitrate-to-sulfate mass ratio decreases rapidly with cloud height, due to the volatilization during drop evaporation pushes NO_3 to the gas phase (Prabhakar et al., 2014). In addition, vertical turbulent mixing of the residual aerosols from evaporating cloud droplets may contribute to the nitrate aerosol loading during the

daytime at the ground level (Tao et al., 2018).

Competing interests

The authors declare that they have no conflict of interest.

Data availability

All the data can be obtained by contacting the corresponding author.

Author contribution

GHZ and XHB designed the research (with input from LL, MT, and XW), analyzed the data (with input from XDH and WS), and wrote the paper. YXY, ZYG, and YZF performed the field measurements and analyzed the collected samples. DHC, HCW, SZZ, and ZBS provided constructive comments. All authors contributed to the refinement of the manuscript.

Acknowledgement

Thanks to Prof. Likun Xue (Shandong University) and Dr. Liang Wen (Leibniz Institute for Tropospheric Research) for their support of the box modeling of nitrate formation in cloud.

Financial support

This work was funded by the Natural Science Foundation of Guangdong Province (2019B151502022), National Natural Science Foundation of China (42077322, 41775124, and 41877307), Youth Innovation Promotion Association CAS (2021354), and Guangdong Foundation for Program of Science and Technology Research (2020B1212060053).

References

Aksoyoglu, S., Ciarelli, G., El-Haddad, I., Baltensperger, U., and Prevot, A. S. H.: Secondary inorganic aerosols in Europe: sources and the significant influence of biogenic VOC emissions, especially on ammonium nitrate, Atmos. Chem. Phys., 17, 7757-7773, doi:10.5194/acp-17-7757-2017, 2017.

Alexander, B., Hastings, M. G., Allman, D. J., Dachs, J., Thornton, J. A., and Kunasek, S. A.: Quantifying atmospheric nitrate formation pathways based on a global model of the oxygen isotopic composition ($\Delta^{17}O$) of atmospheric nitrate, Atmos. Chem. Phys., 9, 5043-5056, doi:10.5194/acp-9-5043-2009, 2009.

Alexander, B., Sherwen, T., Holmes, C. D., Fisher, J. A., Chen, Q., Evans, M. J., and Kasibhatla, P.: Global inorganic nitrate production mechanisms: comparison of a global model with nitrate isotope observations, Atmos. Chem. Phys., 20, 3859-3877, doi:10.5194/acp-20-3859-2020, 2020.

Bauer, S. E., Koch, D., Unger, N., Metzger, S. M., Shindell, D. T., and Streets, D. G.: Nitrate aerosols today and in 2030: a global simulation including aerosols and tropospheric ozone, Atmos. Chem. Phys., 7, 5043-5059, doi:10.5194/acp-7-5043-2007, 2007.

Bertram, T. H., and Thornton, J. A.: Toward a general parameterization of N2O5 reactivity on aqueous particles: the competing effects of particle liquid water, nitrate and chloride, Atmos. Chem. Phys., 9, 8351-8363, doi:10.5194/acp-9-8351-2009, 2009.

Bi, X. H., Lin, Q. H., Peng, L., Zhang, G. H., Wang, X. M., Brechtel, F. J., Chen, D. H., Li, M., Peng, P. A., Sheng, G. Y., and Zhou, Z.: In situ detection of the chemistry of individual fog droplet residues in the Pearl River Delta region, China, J. Geophys. Res.-Atmos., 121, 9105-9116, doi:10.1002/2016JD024886, 2016.

Boone, E. J., Laskin, A., Laskin, J., Wirth, C., Shepson, P. B., Stirm, B. H., and Pratt, K. A.: Aqueous Processing of Atmospheric Organic Particles in Cloud Water Collected via Aircraft Sampling, Environ. Sci. Technol., 49, 8523-8530, doi:10.1021/acs.est.5b01639, 2015.

Brown, S. S., Dube, W. P., Tham, Y. J., Zha, Q. Z., Xue, L. K., Poon, S., Wang, Z., Blake, D. R., Tsui, W., Parrish, D. D., and Wang, T.: Nighttime chemistry at a high altitude site above Hong

Kong, J. Geophys. Res.-Atmos., 121, 2457-2475, doi:10.1002/2015JD024566, 2016.

Burkholder, J. B., Sander, S. P., Abbatt, J., Barker, J. R., Huie, R. E., Kolb, C. E., Kurylo, M. J., Orkin, V. L., Wilmouth, D. M., and Wine, P. H.: Chemical kinetics and photochemical data for use in atmospheric studies C, edited by: Evaluation No. 18, J. P.-. National Aeronautics and Space Administration, http://jpldataeval.jpl.nasa.gov (last access: 10 May 2022), 2015.

Chan, Y.-C., Evans, M. J., He, P., Holmes, C. D., Jaegle, L., Kasibhatla, P., Liu, X.-Y., Sherwen, T., Thornton, J. A., Wang, X., Xie, Z., Zhai, S., and Alexander, B.: Heterogeneous Nitrate Production Mechanisms in Intense Haze Events in the North China Plain, J. Geophys. Res.-Atmos., 126, doi:10.1029/2021jd034688, 2021.

Chang, W. L., Bhave, P. V., Brown, S. S., Riemer, N., Stutz, J., and Dabdub, D.: Heterogeneous Atmospheric Chemistry, Ambient Measurements, and Model Calculations of N2O5: A Review, Aerosol Sci. Tech., 45, 665-695, doi:10.1080/02786826.2010.551672, 2011.

Chen, X., Wang, H., Lu, K., Li, C., Zhai, T., Tan, Z., Ma, X., Yang, X., Liu, Y., Chen, S., Dong, H., Li, X., Wu, Z., Hu, M., Zeng, L., and Zhang, Y.: Field Determination of Nitrate Formation Pathway in Winter Beijing, Environ. Sci. Technol., 54, 9243-9253, doi:10.1021/acs.est.0c00972, 2020.

Chen, Y., Wolke, R., Ran, L., Birmili, W., Spindler, G., Schroder, W., Su, H., Cheng, Y. F., Tegen, I., and Wiedensohler, A.: A parameterization of the heterogeneous hydrolysis of N_2O_5 for mass-based aerosol models: improvement of particulate nitrate prediction, Atmos. Chem. Phys., 18, 673-689, doi:10.5194/acp-18-673-2018, 2018.

Chu, B., Ma, Q., Liu, J., Ma, J., Zhang, P., Chen, T., Feng, Q., Wang, C., Yang, N., Ma, H., Ma, J., Russell, A. G., and He, H.: Air Pollutant Correlations in China: Secondary Air Pollutant Responses to NOx and SO_2 Control, Environ. Sci. Tech. Let., 7, 695-700, doi:10.1021/acs.estlett.0c00403, 2020.

Draxler, R. R., and Rolph, G. D.: HYSPLIT (HYbrid Single-Particle Lagrangian Integrated Trajectory) Model access via NOAA ARL READY Website (http://ready.arl.noaa.gov/HYSPLIT.php), NOAA Air Resources Laboratory, MD, Silver Spring, 2012.

Drewnick, F., Schneider, J., Hings, S. S., Hock, N., Noone, K., Targino, A., Weimer, S., and

Borrmann, S.: Measurement of ambient, interstitial, and residual aerosol particles on a mountaintop site in central Sweden using an aerosol mass spectrometer and a CVI, J. Atmos. Chem., 56, 1-20, doi:10.1007/s10874-006-9036-8, 2007.

Ervens, B., George, C., Williams, J. E., Buxton, G. V., Salmon, G. A., Bydder, M., Wilkinson, F., Dentener, F., Mirabel, P., Wolke, R., and Herrmann, H.: CAPRAM 2.4 (MODAC mechanism): An extended and condensed tropospheric aqueous phase mechanism and its application, J. Geophys. Res.-Atmos., 108, doi:10.1029/2002jd002202, 2003.

Ervens, B.: Modeling the Processing of Aerosol and Trace Gases in Clouds and Fogs, Chem. Rev., 115, 4157-4198, doi:10.1021/cr5005887, 2015.

Fahey, K. M., Pandis, S. N., Collett, J. L., and Herckes, P.: The influence of size-dependent droplet composition on pollutant processing by fogs, Atmos. Environ., 39, 4561-4574, doi:10.1016/j.atmosenv.2005.04.006, 2005.

Fan, M. Y., Zhang, Y. L., Lin, Y. C., Hong, Y., Zhao, Z. Y., Xie, F., Du, W., Cao, F., Sun, Y., and Fu, P.: Important Role of NO3 Radical to Nitrate Formation Aloft in Urban Beijing: Insights from Triple Oxygen Isotopes Measured at the Tower, Environ. Sci. Technol., doi:10.1021/acs.est.1c02843, 2021.

Fu, X., Wang, T., Gao, J., Wang, P., Liu, Y., Wang, S., Zhao, B., and Xue, L.: Persistent Heavy Winter Nitrate Pollution Driven by Increased Photochemical Oxidants in Northern China, Environ. Sci. Technol., 54, 3881-3889, doi:10.1021/acs.est.9b07248, 2020.

Guo, S., Hu, M., Zamora, M. L., Peng, J., Shang, D., Zheng, J., Du, Z., Wu, Z., Shao, M., Zeng, L., Molina, M. J., and Zhang, R.: Elucidating severe urban haze formation in China, Proc. Natl. Acad. Sci. USA, 111, 17373, doi:10.1073/pnas.1419604111, 2014.

Hall, S. R., Ullmann, K., Prather, M. J., Flynn, C. M., Murray, L. T., Fiore, A. M., Correa, G., Strode, S. A., Steenrod, S. D., Lamarque, J.-F., Guth, J., Josse, B., Flemming, J., Huijnen, V., Abraham, N. L., and Archibald, A. T.: Cloud impacts on photochemistry: building a climatology of photolysis rates from the Atmospheric Tomography mission, Atmos. Chem. Phys., 18, 16809-16828, doi:10.5194/acp-18-16809-2018, 2018.

Hao, L., Romakkaniemi, S., Kortelainen, A., Jaatinen, A., Portin, H., Miettinen, P., Komppula, M., Leskinen, A., Virtanen, A., Smith, J. N., Sueper, D., Worsnop, D. R., Lehtinen, K. E. J., and

509 Laaksonen, A.: Aerosol Chemical Composition in Cloud Events by High Resolution Time-of-
510 Flight Aerosol Mass Spectrometry, Environ. Sci. Technol., 47, 2645-2653,
511 doi:10.1021/es302889w, 2013.
512 Hauglustaine, D. A., Balkanski, Y., and Schulz, M.: A global model simulation of present and
513 future nitrate aerosols and their direct radiative forcing of climate, Atmos. Chem. Phys., 14,
514 11031-11063, doi:10.5194/acp-14-11031-2014, 2014.
515 Hayden, K. L., Macdonald, A. M., Gong, W., Toom-Sauntry, D., Anlauf, K. G., Leithead, A., Li,
516 S. M., Leaitch, W. R., and Noone, K.: Cloud processing of nitrate, J. Geophys. Res.-Atmos.,
517 113, 1-18, doi:10.1029/2007jd009732, 2008.
518 Healy, R. M., Sciare, J., Poulain, L., Crippa, M., Wiedensohler, A., Prevot, A. S. H.,
519 Baltensperger, U., Sarda-Esteve, R., McGuire, M. L., Jeong, C. H., McGillicuddy, E., O'Connor,
520 I. P., Sodeau, J. R., Evans, G. J., and Wenger, J. C.: Quantitative determination of carbonaceous
521 particle mixing state in Paris using single-particle mass spectrometer and aerosol mass
522 spectrometer measurements, Atmos. Chem. Phys., 13, 9479-9496, doi:10.5194/acp-13-9479-
523 2013, 2013.
524 Herckes, P., Chang, H., Lee, T., and Collett, J. L.: Air pollution processing by radiation fogs,
525 Water Air Soil Pollut., 181, 65-75, doi:10.1007/s11270-006-9276-x, 2007.
526 Herckes, P., Marcotte, A. R., Wang, Y., and Collett, J. L.: Fog composition in the Central Valley
527 of California over three decades, Atmos. Res., 151, 20-30, doi:10.1016/j.atmosres.2014.01.025,
528 2015.
529 Hodas, N., Sullivan, A. P., Skog, K., Keutsch, F. N., Collett, J. L., Jr., Decesari, S., Facchini, M.
530 C., Carlton, A. G., Laaksonen, A., and Turpin, B. J.: Aerosol liquid water driven by
531 anthropogenic nitrate: implications for lifetimes of water-soluble organic gases and potential for
532 secondary organic aerosol formation, Environ. Sci. Technol., 48, 11127-11136,
533 doi:10.1021/es5025096, 2014.
534 Holmes, C. D., Bertram, T. H., Confer, K. L., Grahams, K. A., Ronan, A. C., Wirks, C. K., and
535 Shah, V.: The Role of Clouds in the Tropospheeric NOx Cycle: A New Modeling Approach for
536 Cloud Chemistry and Its Global Implications, Geophys. Res. Lett., 46, 4980-4990,
537 doi:10.1029/2019gl081990, 2019.

Huang, D. D., Zhang, Q., Cheung, H. H. Y., Yu, L., Zhou, S., Anastasio, C., Smith, J. D., and Chan, C. K.: Formation and Evolution of aqSOA from Aqueous-Phase Reactions of Phenolic Carbonyls: Comparison between Ammonium Sulfate and Ammonium Nitrate Solutions, Environ. Sci. Technol., 52, 9215-9224, doi:10.1021/acs.est.8b03441, 2018.

Jeong, C. H., McGuire, M. L., Godri, K. J., Slowik, J. G., Rehbein, P. J. G., and Evans, G. J.: Quantification of aerosol chemical composition using continuous single particle measurements, Atmos. Chem. Phys., 11, 7027-7044, doi:10.5194/acp-11-7027-2011, 2011.

Kaur, R., and Anastasio, C.: Light absorption and the photoformation of hydroxyl radical and singlet oxygen in fog waters, Atmos. Environ., 164, 387-397, doi:10.1016/j.atmosenv.2017.06.006, 2017.

Leaitch, W. R., Bottenheim, J. W., and Strapp, J. W.: Possible contribution of N_2O_5 scavenging to HNO_3 observed in winter stratiform cloud, J. Geophys. Res.-Atmos., 93, 12569-12584, doi:10.1029/JD093iD10p12569, 1988.

Li, H. Y., Zhang, Q., Zheng, B., Chen, C. R., Wu, N. N., Guo, H. Y., Zhang, Y. X., Zheng, Y. X., Li, X., and He, K. B.: Nitrate-driven urban haze pollution during summertime over the North China Plain, Atmos. Chem. Phys., 18, 5293-5306, doi:10.5194/acp-18-5293-2018, 2018.

Li, L., Huang, Z. X., Dong, J. G., Li, M., Gao, W., Nian, H. Q., Fu, Z., Zhang, G. H., Bi, X. H., Cheng, P., and Zhou, Z.: Real time bipolar time-of-flight mass spectrometer for analyzing single aerosol particles, Intl. J. Mass. Spectrom., 303, 118-124, doi:10.1016/j.ijms.2011.01.017, 2011.

Li, S., Zhang, F., Jin, X., Sun, Y., Wu, H., Xie, C., Chen, L., Liu, J., Wu, T., Jiang, S., Cribb, M., and Li, Z.: Characterizing the ratio of nitrate to sulfate in ambient fine particles of urban Beijing during 2018–2019, Atmos. Environ., 117662, doi:10.1016/j.atmosenv.2020.117662, 2020a.

Li, T., Wang, Z., Wang, Y. R., Wu, C., Liang, Y. H., Xia, M., Yu, C., Yun, H., Wang, W. H., Wang, Y., Guo, J., Herrmann, H., and Wang, T.: Chemical characteristics of cloud water and the impacts on aerosol properties at a subtropical mountain site in Hong Kong SAR, Atmos. Chem. Phys., 20, 391-407, doi:10.5194/acp-20-391-2020, 2020b.

Lin, Q., Zhang, G., Peng, L., Bi, X., Wang, X., Brechtel, F. J., Li, M., Chen, D., Peng, P. a., Sheng, G., and Zhou, Z.: In situ chemical composition measurement of individual cloud residue particles at a mountain site, southern China, Atmos. Chem. Phys., 17, 8473-8488,

567 doi:10.5194/acp-17-8473-2017, 2017.
568 Lin, Y. C., Zhang, Y. L., Yu, M., Fan, M. Y., Xie, F., Zhang, W. Q., Wu, G., Cong, Z., and
569 Michalski, G.: Formation Mechanisms and Source Apportionments of Airborne Nitrate
570 Aerosols at a Himalayan-Tibetan Plateau Site: Insights from Nitrogen and Oxygen Isotopic
571 Compositions, Environ. Sci. Technol., 55, 12261-12271, doi:10.1021/acs.est.1c03957, 2021.
572 Liu, H. Y., Crawford, J. H., Pierce, R. B., Norris, P., Platnick, S. E., Chen, G., Logan, J. A.,
573 Yantosca, R. M., Evans, M. J., Kittaka, C., Feng, Y., and Tie, X. X.: Radiative effect of clouds
574 on tropospheric chemistry in a global three-dimensional chemical transport model, J. Geophys.
575 Res.-Atmos., 111, 18, doi:10.1029/2005jd006403, 2006.
576 Liu, L., Bei, N. F., Hu, B., Wu, J. R., Liu, S. X., Li, X., Wang, R. N., Liu, Z. R., Shen, Z. X.,
577 and Li, G. H.: Wintertime nitrate formation pathways in the north China plain: Importance of
578 N2O5 heterogeneous hydrolysis, Environ. Pollut., 266, 10, doi:10.1016/j.envpol.2020.115287,
579 2020a.
580 Liu, P., Ye, C., Xue, C., Zhang, C., Mu, Y., and Sun, X.: Formation mechanisms of atmospheric
581 nitrate and sulfate during the winter haze pollution periods in Beijing: gas-phase, heterogeneous
582 and aqueous-phase chemistry, Atmos. Chem. Phys., 20, 4153-4165, doi:10.5194/acp-20-4153-
583 2020, 2020b.
584 Lu, K., Fuchs, H., Hofzumahaus, A., Tan, Z., Wang, H., Zhang, L., Schmitt, S. H., Rohrer, F.,
585 Bohn, B., Broch, S., Dong, H., Gkatzelis, G. I., Hohaus, T., Holland, F., Li, X., Liu, Y., Liu, Y.,
586 Ma, X., Novelli, A., Schlag, P., Shao, M., Wu, Y., Wu, Z., Zeng, L., Hu, M., Kiendler-Scharr,
587 A., Wahner, A., and Zhang, Y.: Fast Photochemistry in Wintertime Haze: Consequences for
588 Pollution Mitigation Strategies, Environ. Sci. Technol., 53, 10676-10684,
589 doi:10.1021/acs.est.9b02422, 2019.
590 McNeill, V. F.: Atmospheric Aerosols: Clouds, Chemistry, and Climate, Annu. Rev. Chem.
591 Biomol., 8, 427-444, doi:10.1146/annurev-chembioeng-060816-101538, 2017.
592 Neuman, J. A., Nowak, J. B., Brock, C. A., Trainer, M., Fehsenfeld, F. C., Holloway, J. S.,
593 Hubler, G., Hudson, P. K., Murphy, D. M., Nicks, D. K., Orsini, D., Parrish, D. D., Ryerson, T.
594 B., Sueper, D. T., Sullivan, A., and Weber, R.: Variability in ammonium nitrate formation and
595 nitric acid depletion with altitude and location over California, J. Geophys. Res.-Atmos., 108,

12, doi:10.1029/2003jd003616, 2003.

Pathak, R. K., Wu, W. S., and Wang, T.: Summertime $PM_{2.5}$ ionic species in four major cities of China: nitrate formation in an ammonia-deficient atmosphere, Atmos. Chem. Phys., 9, 1711-1722, 2009.

Prabhakar, G., Ervens, B., Wang, Z., Maudlin, L. C., Coggon, M. M., Jonsson, H. H., Seinfeld, J. H., and Sorooshian, A.: Sources of nitrate in stratocumulus cloud water: Airborne measurements during the 2011 E-PEACE and 2013 NiCE studies, Atmos. Environ., 97, 166-173, doi:10.1016/j.atmosenv.2014.08.019, 2014.

Pratt, K. A., DeMott, P. J., French, J. R., Wang, Z., Westphal, D. L., Heymsfield, A. J., Twohy, C. H., Prenni, A. J., and Prather, K. A.: In situ detection of biological particles in cloud ice-crystals, Nature Geosci., 2, 397-400, 2009.

Qu, K., Wang, X., Xiao, T., Shen, J., Lin, T., Chen, D., He, L.-Y., Huang, X.-F., Zeng, L., Lu, K., Ou, Y., and Zhang, Y.: Cross-regional transport of $PM_{2.5}$ nitrate in the Pearl River Delta, China: Contributions and mechanisms, Sci. Total. Environ., 753, doi:10.1016/j.scitotenv.2020.142439, 2021.

Riemer, N., Vogel, H., Vogel, B., Schell, B., Ackermann, I., Kessler, C., and Hass, H.: Impact of the heterogeneous hydrolysis of N_2O_5 on chemistry and nitrate aerosol formation in the lower troposphere under photosmog conditions, J. Geophys. Res.-Atmos., 108, 21, doi:10.1029/2002jd002436, 2003.

Roth, A., Schneider, J., Klimach, T., Mertes, S., van Pinxteren, D., Herrmann, H., and Borrmann, S.: Aerosol properties, source identification, and cloud processing in orographic clouds measured by single particle mass spectrometry on a central European mountain site during HCCT-2010, Atmos. Chem. Phys., 16, 505-524, doi:10.5194/acp-16-505-2016, 2016.

Scharko, N. K., Berke, A. E., and Raff, J. D.: Release of Nitrous Acid and Nitrogen Dioxide from Nitrate Photolysis in Acidic Aqueous Solutions, Environ. Sci. Technol., 48, 11991-12001, doi:10.1021/es503088x, 2014.

Schneider, J., Mertes, S., van Pinxteren, D., Herrmann, H., and Borrmann, S.: Uptake of nitric acid, ammonia, and organics in orographic clouds: mass spectrometric analyses of droplet residual and interstitial aerosol particles, Atmos. Chem. Phys., 17, 1571-1593, doi:10.5194/acp-

17-1571-2017, 2017.

Seinfeld, J. H., and Pandis, S. N.: Atmospheric Chemistry and Physics: From Air Pollution to Climate Change, edited by: John Wiley&Sons, I., John Wiley&Sons, Inc., New Jersey, 2006.

Sellegri, K., Laj, P., Marinoni, A., Dupuy, R., Legrand, M., and Preunkert, S.: Contribution of gaseous and particulate species to droplet solute composition at the Puy de Dome, France, Atmos. Chem. Phys., 3, 1509-1522, doi:10.5194/acp-3-1509-2003, 2003.

Shi, X., Nenes, A., Xiao, Z., Song, S., Yu, H., Shi, G., Zhao, Q., Chen, K., Feng, Y., and Russell, A. G.: High-Resolution Data Sets Unravel the Effects of Sources and Meteorological Conditions on Nitrate and Its Gas-Particle Partitioning, Environ. Sci. Technol., 53, 3048-3057, doi:10.1021/acs.est.8b06524, 2019.

Shingler, T., Dey, S., Sorooshian, A., Brechtel, F. J., Wang, Z., Metcalf, A., Coggon, M., Mulmenstadt, J., Russell, L. M., Jonsson, H. H., and Seinfeld, J. H.: Characterisation and airborne deployment of a new counterflow virtual impactor inlet, Atmos. Meas. Tech., 5, 1259-1269, doi:10.5194/amt-5-1259-2012, 2012.

Song, X. H., Hopke, P. K., Fergenson, D. P., and Prather, K. A.: Classification of single particles analyzed by ATOFMS using an artificial neural network, ART-2A, Anal. Chem., 71, 860-865, 1999.

Strode, S. A., Douglass, A. R., Ziemke, J. R., Manyin, M., Nielsen, J. E., and Oman, L. D.: A Model and Satellite-Based Analysis of the Tropospheric Ozone Distribution in Clear Versus Convectively Cloudy Conditions, J. Geophys. Res.-Atmos., 122, 11948-11960, doi:10.1002/2017jd027015, 2017.

Sultana, C. M., Cornwell, G. C., Rodriguez, P., and Prather, K. A.: FATES: a flexible analysis toolkit for the exploration of single-particle mass spectrometer data, Atmos. Meas. Tech., 10, 1323-1334, doi:10.5194/amt-10-1323-2017, 2017.

Sun, J. X., Liu, L., Xu, L., Wang, Y. Y., Wu, Z. J., Hu, M., Shi, Z. B., Li, Y. J., Zhang, X. Y., Chen, J. M., and Li, W. J.: Key Role of Nitrate in Phase Transitions of Urban Particles: Implications of Important Reactive Surfaces for Secondary Aerosol Formation, J. Geophys. Res.-Atmos., 123, 1234-1243, doi:10.1002/2017JD027264, 2018.

Tao, J., Zhang, Z., Tan, H., Zhang, L., Wu, Y., Sun, J., Che, H., Cao, J., Cheng, P., Chen, L., and

Zhang, R.: Observational evidence of cloud processes contributing to daytime elevated nitrate in an urban atmosphere, Atmos. Environ., 186, 209-215, doi:10.1016/j.atmosenv.2018.05.040, 2018.

Tian, M., Liu, Y., Yang, F. M., Zhang, L. M., Peng, C., Chen, Y., Shi, G. M., Wang, H. B., Luo, B., Jiang, C. T., Li, B., Takeda, N., and Koizumi, K.: Increasing importance of nitrate formation for heavy aerosol pollution in two megacities in Sichuan Basin, southwest China, Environ. Pollut., 250, 898-905, doi:10.1016/j.envpol.2019.04.098, 2019.

Voulgarakis, A., Wild, O., Savage, N. H., Carver, G. D., and Pyle, J. A.: Clouds, photolysis and regional tropospheric ozone budgets, Atmos. Chem. Phys., 9, 8235-8246, doi:10.5194/acp-9-8235-2009, 2009.

Wang, H., Lu, K., Chen, X., Zhu, Q., Chen, Q., Guo, S., Jiang, M., Li, X., Shang, D., Tan, Z., Wu, Y., Wu, Z., Zou, Q., Zheng, Y., Zeng, L., Zhu, T., Hu, M., and Zhang, Y.: High N_2O_5 Concentrations Observed in Urban Beijing: Implications of a Large Nitrate Formation Pathway, Environ. Sci. Tech. Let., doi:10.1021/acs.estlett.7b00341, 2017.

Wang, X. F., Zhang, Y. P., Chen, H., Yang, X., Chen, J. M., and Geng, F. H.: Particulate Nitrate Formation in a Highly Polluted Urban Area: A Case Study by Single-Particle Mass Spectrometry in Shanghai, Environ. Sci. Technol., 43, 3061-3066, doi:10.1021/es8020155, 2009.

Wen, L., Xue, L. K., Wang, X. F., Xu, C. H., Chen, T. S., Yang, L. X., Wang, T., Zhang, Q. Z., and Wang, W. X.: Summertime fine particulate nitrate pollution in the North China Plain: increasing trends, formation mechanisms and implications for control policy, Atmos. Chem. Phys., 18, 11261-11275, doi:10.5194/acp-18-11261-2018, 2018.

Wu, C., Liu, L., Wang, G., Zhang, S., Li, G., Lv, S., Li, J., Wang, F., Meng, J., and Zens, Y.: Important contribution of N_2O_5 hydrolysis to the daytime nitrate in Xi'an, China during haze periods: Isotopic analysis and WRF-Chem model simulation, Environ. Pollut., 117712, doi:10.1016/j.envpol.2021.117712, 2021.

Xiao, H.-W., Zhu, R.-G., Pan, Y.-Y., Guo, W., Zheng, N.-J., Liu, Y.-H., Liu, C., Zhang, Z.-Y., Wu, J.-F., Kang, C.-A., Luo, L., and Xiao, H.-Y.: Differentiation Between Nitrate Aerosol Formation Pathways in a Southeast Chinese City by Dual Isotope and Modeling Studies, J.

Geophys. Res.-Atmos., 125, doi:10.1029/2020jd032604, 2020.

Xu, L., and Penner, J. E.: Global simulations of nitrate and ammonium aerosols and their radiative effects, Atmos. Chem. Phys., 12, 9479-9504, doi:10.5194/acp-12-9479-2012, 2012.

Xu, Q., Wang, S., Jiang, J., Bhattarai, N., Li, X., Chang, X., Qiu, X., Zheng, M., Hua, Y., and Hao, J.: Nitrate dominates the chemical composition of $PM_{2.5}$ during haze event in Beijing, China, Sci. Total. Environ., 689, 1293-1303, doi:10.1016/j.scitotenv.2019.06.294, 2019.

Yan, C., Tham, Y. J., Zha, Q. Z., Wang, X. F., Xue, L. K., Dai, J. N., Wang, Z., and Wang, T.: Fast heterogeneous loss of N_2O_5 leads to significant nighttime NOx removal and nitrate aerosol formation at a coastal background environment of southern China, Sci. Total. Environ., 677, 637-647, doi:10.1016/j.scitotenv.2019.04.389, 2019.

Ye, C., Heard, D. E., and Whalley, L. K.: Evaluation of Novel Routes for NOx Formation in Remote Regions, Environ. Sci. Technol., 51, 7442-7449, doi:10.1021/acs.est.6b06441, 2017a.

Ye, C., Zhang, N., Gao, H., and Zhou, X.: Photolysis of Particulate Nitrate as a Source of HONO and NOx, Environ. Sci. Technol., 51, 6849-6856, doi:10.1021/acs.est.7b00387, 2017b.

Zhai, S., Jacob, D. J., Wang, X., Liu, Z., Wen, T., Shah, V., Li, K., Moch, J. M., Bates, K. H., Song, S., Shen, L., Zhang, Y., Luo, G., Yu, F., Sun, Y., Wang, L., Qi, M., Tao, J., Gui, K., Xu, H., Zhang, Q., Zhao, T., Wang, Y., Lee, H. C., Choi, H., and Liao, H.: Control of particulate nitrate air pollution in China, Nature Geosci., 14, 389-395, doi:10.1038/s41561-021-00726-z, 2021.

Zhang, G. H., Lin, Q. H., Peng, L., Yang, Y. X., Fu, Y. Z., Bi, X. H., Li, M., Chen, D. H., Chen, J. X., Cai, Z., Wang, X. M., Peng, P. A., Sheng, G. Y., and Zhou, Z.: Insight into the in-cloud formation of oxalate based on in situ measurement by single particle mass spectrometry, Atmos. Chem. Phys., 17, 13891-13901, doi:10.5194/acp-17-13891-2017, 2017.

Zhang, J., Lance, S., Brandt, R., Marto, J., Ninneman, M., and Schwab, J.: Observed below-Cloud and Cloud Interstitial Submicron Aerosol Chemical and Physical Properties at Whiteface Mountain, New York, during August 2017, Acs Earth Space Chem., 3, 1438-1450, doi:10.1021/acsearthspacechem.9b00117, 2019.

Zhang, R., Gen, M., Fu, T. M., and Chan, C. K.: Production of Formate via Oxidation of Glyoxal Promoted by Particulate Nitrate Photolysis, Environ. Sci. Technol., 55, 5711-5720,

doi:10.1021/acs.est.0c08199, 2021.

Zheng, H., Song, S., Sarwar, G., Gen, M., Wang, S., Ding, D., Chang, X., Zhang, S., Xing, J., Sun, Y., Ji, D., Chan, C. K., Gao, J., and McElroy, M. B.: Contribution of Particulate Nitrate Photolysis to Heterogeneous Sulfate Formation for Winter Haze in China, Environ. Sci. Tech. Let., 7, 632-638, doi:10.1021/acs.estlett.0c00368, 2020.

Zhu, Y., Tilgner, A., Hoffmann, E. H., Herrmann, H., Kawamura, K., Yang, L., Xue, L., and Wang, W.: Multiphase MCM-CAPRAM modeling of the formation and processing of secondary aerosol constituents observed during the Mt. Tai summer campaign in 2014, Atmos. Chem. Phys., 20, 6725-6747, doi:10.5194/acp-20-6725-2020, 2020.

Figure captions:

Figure 1. Box-and-whisker plots of (a) the mass fraction of nitrate in $PM_{2.5}$ and cloud water and (b) the RPA of nitrate separated for the cloud-free, cloud residual (RES), and cloud interstitial (INT) particles, in 2018 spring and 2020 winter, respectively. In a box and whisker plot, the lower, median and upper line of the box denotes the 25, 50, and 75 percentiles, respectively; the lower and upper edges of the whisker denote the 10 and 90 percentiles, respectively.

Figure 2. Size dependent RPA of nitrate and RPA ratio of nitrate/sulfate, separated for all the detected cloud-free, cloud residual (RES), and cloud interstitial (INT) particles, in (a) 2018 spring (May) and (b) 2020 winter (Nov-Dec), respectively.

Figure 3. Theoretical calculation of the trend of in-cloud produced nitrate from the hydrolysis of N_2O_5 versus the temporal variations of NO_3^- concentration in cloud water in 2020 winter (Nov-Dec).

Figure 4. Correlation analysis between the observed RPAs of nitrate and the predicted RPAs of nitrate, with inputs of NO_2, O_3 and LWC, for the (a) cloud-free and (b) cloud RES particles, respectively.

Figure 5. Relative contribution of each pathway to the nitrate production in wet aerosols (WA, 0.5 μm) and cloud droplets (CD, 8 μm), respectively, simulated by the RACM-CAPRAM. The atmospheric conditions considered for comparison are LWC

741 (10^{-5}-10^{-4} g cm^{-3} for wet aerosols and 0.05-0.15 g cm^{-3}) and photolysis rates (30%,

742 50%, 100%).

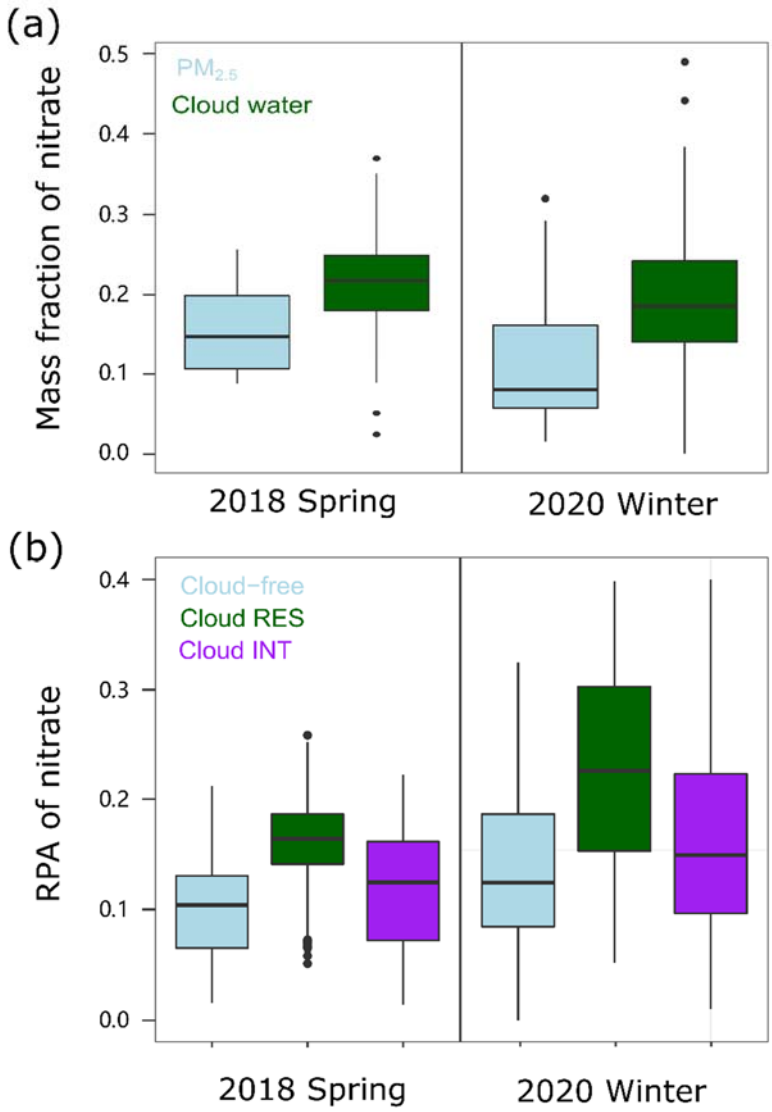
(a)
Mass fraction of nitrate
0.5
0.4
0.3
0.2
0.1
0.0
PM2.5
Cloud water
2018 Spring
2020 Winter
(b)
RPA of nitrate
0.4
0.3
0.2
0.1
0.0
Cloud−free
Cloud RES
Cloud INT
2018 Spring
2020 Winter

743

744 **Fig. 1.**

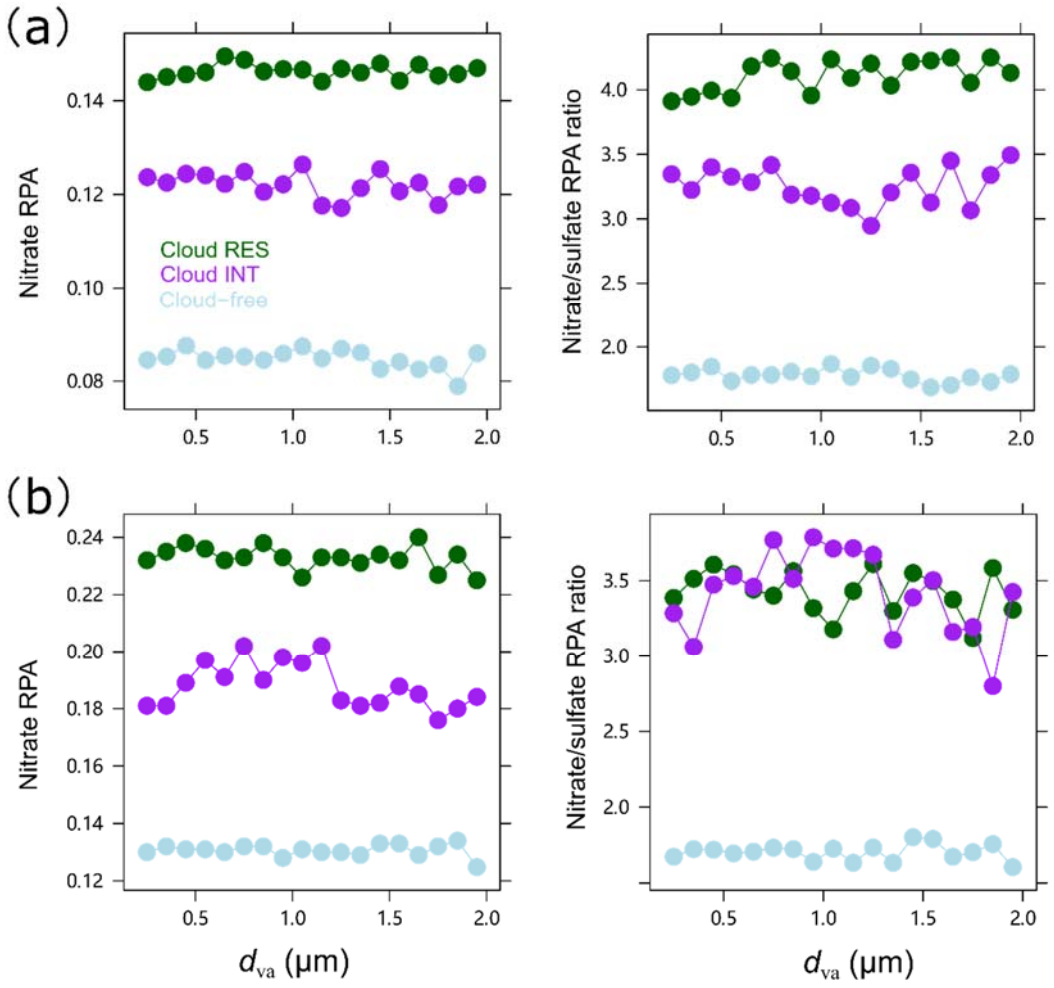
(a)
(b)
Nitrate RPA
Nitrate/sulfate RPA ratio
Cloud RES
Cloud INT
Cloud−free
d_{va} (μm)
d_{va} (μm)

745

746 **Fig. 2.**

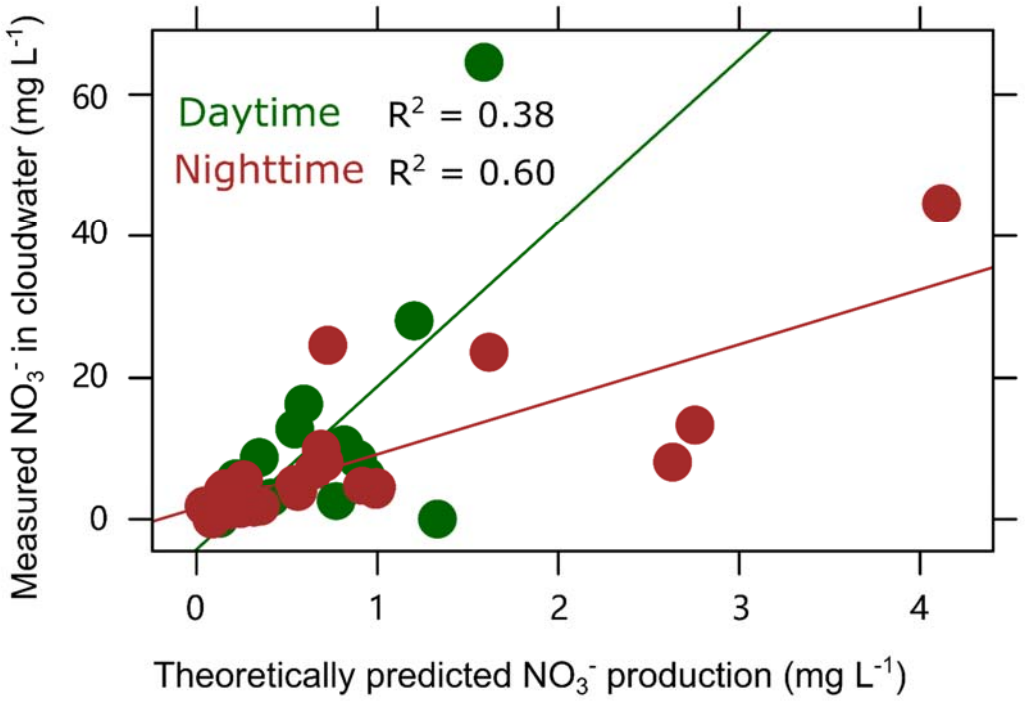
Daytime R² = 0.38
Nighttime R² = 0.60
Measured NO3- in cloudwater (mg L-1)
Theoretically predicted NO3- production (mg L-1)
0
20
40
60
0
1
2
3
4

747

748 **Fig. 3.**

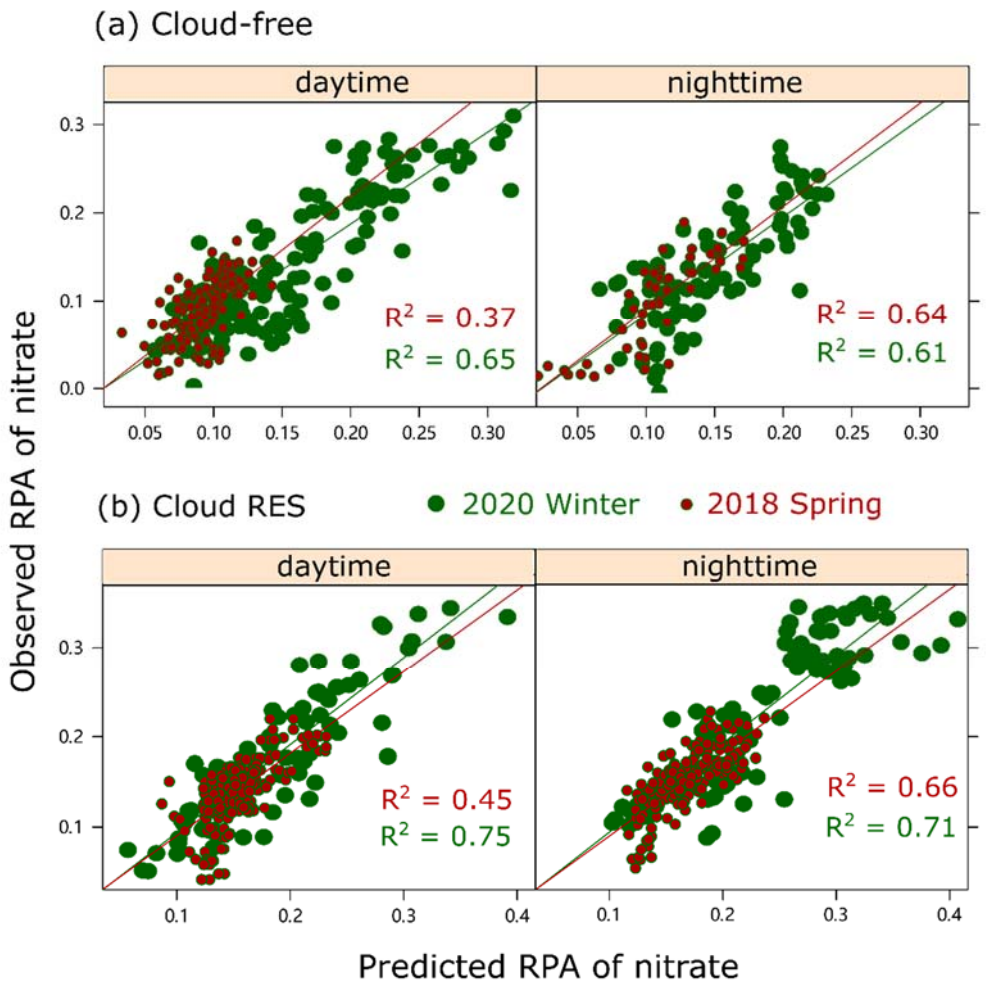
(a) Cloud-free
daytime
nighttime
R² = 0.37
R² = 0.65
R² = 0.64
R² = 0.61
(b) Cloud RES
2020 Winter
2018 Spring
daytime
nighttime
R² = 0.45
R² = 0.75
R² = 0.66
R² = 0.71
Observed RPA of nitrate
Predicted RPA of nitrate

749

750 **Fig. 4.**

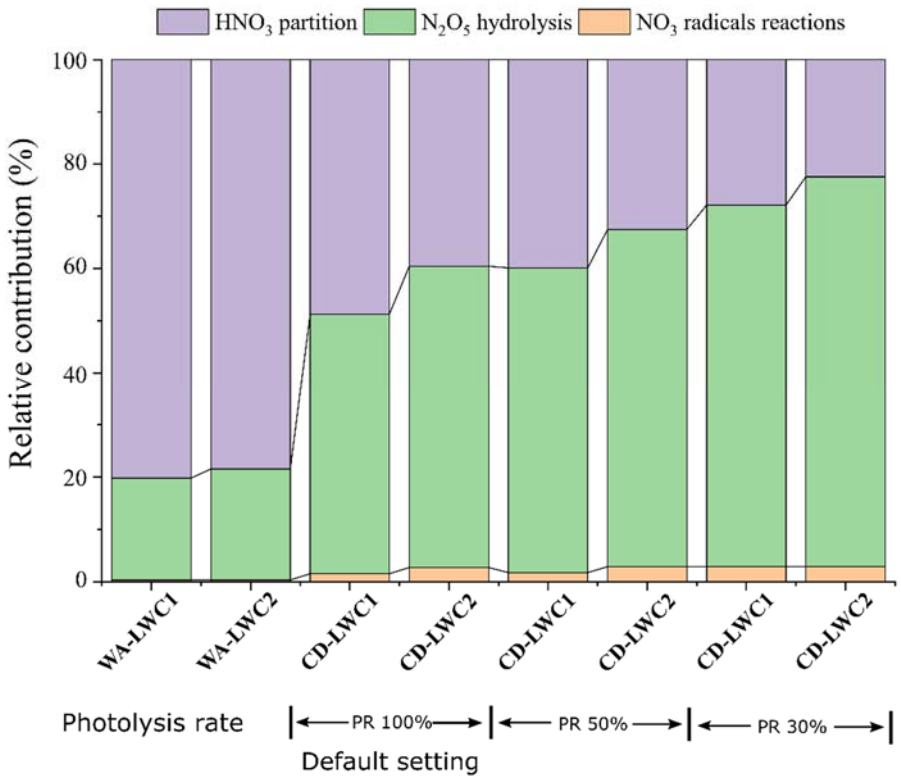
HNO3 partition
N2O5 hydrolysis
NO3 radicals reactions
Relative contribution (%)
100
80
60
40
20
0
WA-LWC1
WA-LWC2
CD-LWC1
CD-LWC2
CD-LWC1
CD-LWC2
CD-LWC1
CD-LWC2
Photolysis rate
PR 100%
PR 50%
PR 30%
Default setting

751

752 **Fig. 5.**